Proceedings of the ASME 2019
International Mechanical Engineering Congress and Exposition
IMECE2019
November 11-14, 2019, Salt Lake City, UT, USA

IMECE2019-10881

NUMERICAL INVESTIGATION OF NONLINEAR LAMB WAVE TIME REVERSING FOR FATIGUE CRACK DETECTION

Junzhen Wang, Yanfeng Shen[1]
University of Michigan-Shanghai Jiao Tong University
Joint Institute, Shanghai Jiao Tong University
Shanghai, China

ABSTRACT

This paper presents a numerical study on nonlinear Lamb wave time reversing for fatigue crack detection. An analytical framework is initially presented, modeling Lamb wave generation, propagation, wave crack linear and nonlinear interaction, and reception. Subsequently, a 3D transient dynamic coupled-field finite element model is constructed to simulate the pitch-catch procedure in an aluminum plate using the commercial finite element software (ANSYS). The excitation frequency is carefully selected, where only single Lamb wave mode will be generated by the Piezoelectric Wafer Active Sensor (PWAS). The fatigue cracks are modelled nucleating from both sides of a rivet hole. In addition, contact dynamics are considered to capture the nonlinear interactions between guided waves and the fatigue cracks, which would induce Contact Acoustic Nonlinearity (CAN) into the guided waves. Then the conventional and virtual time reversal methods are realized by finite element simulation. Advanced signal processing techniques are used to extract the distinctive nonlinear features. Via the Fast Fourier Transform (FFT) and time-frequency spectral analysis, nonlinear superharmonic components are observed. The reconstructed signals attained from the conventional and virtual time reversal methods are compared and analyzed. Finally, various Damage Indices (DIs), based on the difference between the reconstructed signal and the excitation waveform as well as the amplitude ratio between the superharmonic and the fundamental frequency components are adopted to evaluate the fatigue crack severity. The DIs could provide quantitative diagnostic information for fatigue crack detection. This paper finishes with summary, concluding remarks, and suggestions for future work.

Keywords: Lamb waves, time reversal, fatigue crack, damage detection, nonlinear ultrasonics, structural health monitoring

1. INTRODUCTION

Fatigue cracks exist as great menace to engineering structures, because they are barely visible and hard to detect. Thus, the development of effective fatigue crack detection methodologies is of critical importance. Among current solutions, ultrasonic inspection technology has been found to be promising. Compared with linear ultrasonic technologies, the nonlinear ultrasonic counterparts are more sensitive to incipient cracks. The distinctive nonlinear features include but not limited to higher harmonic or subharmonic generation, mixed frequency responses, and nonlinear resonance frequency shift [1]. As an example, Shen et al. investigated the nonlinear resonance phenomenon considering the rough contact surface condition of fatigue cracks [2]. Other efforts have also been exerted on taking advantage of these nonlinear features, including structural inspection techniques considering Contact Acoustic Nonlinearity (CAN), nonlinear surface waves, dual frequency mixing, and time reversal.

The Lamb wave time reversal method has widely been investigated as a baseline-free damage detection technique for Structural Health Monitoring (SHM). To reduce the practical hardware manipulation, Virtual Time Reversal (VTR) algorithm was proposed, which replaces the time reversal procedure by computerized virtual signal operations [3, 4]. The majority of time reversal methods focus on the linear interaction between guided waves and structural damage, such as notch, material loss and erosion [5]. On the other hand, only a few research efforts have been conducted to investigate the nonlinear time reversal techniques for nonlinear damage detection. Ulrich et al. utilized the time reversal method to probe the nonlinear elastic response of diffusion bonds [6]. In addition, nonlinear time reversal and decomposition of time reversal operator (DORT) method were combined for nonlinear elastic damage imaging [7, 8]. The time reversal invariance of ultrasonic plane wave was investigated for a nonlinear scatterer exhibiting CAN [9]. Blanloeuil found that

[1] Contact author: yanfeng.shen@sjtu.edu.cn

the condition to ensure the time reversal invariance is to reemit the new frequency components captured in the forward propagation. Hong et al. used the temporal signal features of nonlinear Lamb waves for fatigue crack imaging by selecting particular excitation frequency for group velocity matching [10]. However, the wave form based nonlinear Lamb wave time reversal procedure was seldom investigated in both three-dimensional numerical simulation and practical experiment. Therefore, this study aims to employ the Lamb wave time reversal methods for fatigue crack detection considering CAN during wave crack interactions. Both temporal and spectral information of nonlinear Lamb waves are synthetically exploited to detect and monitor fatigue cracks.

This study starts with a 2D analytical framework for the efficient modeling of Lamb wave generation, propagation, linear and nonlinear wave damage interaction, and reception. Then, a 3D transient finite element model is constructed for realizing the time reversal process inducing CAN into the guided waves. On the other hand, the VTR algorithm will be applied based on the first pitch-catch active sensing signal. By comparing the results from both traditional and virtual time reversal methods, nonlinear features can be extracted for improved fatigue crack detection performance.

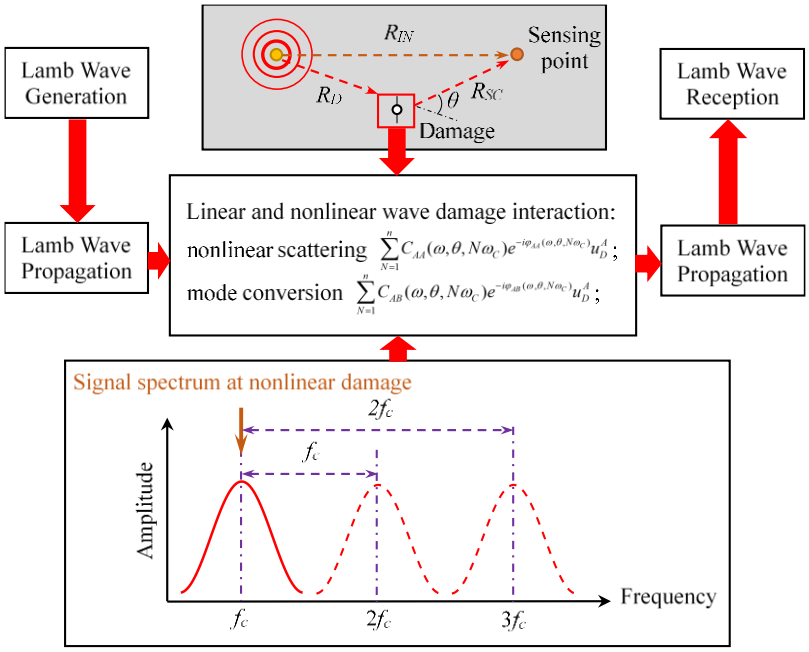

FIGURE 1: ANALYTICAL FRAMEWORK OF THE 2D NONLINEAR LAMB WAVE ACTIVE SENSING PROCEDURE

2. 2D ANALYTICAL FRAMEWORK FOR LAMB WAVE ACTIVE SENSING

This section illustrates the analytical model for Lamb wave active sensing. The analytical formulations of Lamb wave active sensing are first deduced step by step, and then the results of wave propagation for both pristine, linear wave damage interaction, and nonlinear wave damage cases are presented and compared.

2.1 Analytical Model of Lamb Wave Active Sensing

The analytical solution for Lamb wave active sensing using PWAS transducers has been investigated in several existing literatures [4, 11, 12]. Shen and Giurgiutiu developed the WaveFormRevealer, which presents the 1D analytical model including Lamb wave transmission, reflection, mode conversion, and nonlinear higher harmonic generation [11]. Thereafter, they proposed the Combined Analytical Finite Element Model (FEM) Approach (CAFA) for the accurate, efficient and versatile simulation of 2D Lamb wave propagation and linear interaction with structural damage. Based on these pioneer works, the nonlinear interactions between Lamb waves and damage is introduced into the 2D analytical model. In this way, 2D analytical model has been extended and is capable of simulating three scenarios, the pristine case, the linear wave damage interaction case, and the nonlinear wave damage interaction case. Therefore, the new Lamb wave active sensing model can effectively capture all the important elements, including Lamb wave generation, propagation, linear and nonlinear wave damage interaction, and reception.

2.2 2D Analytical Framework Construction

The analytical framework for PWAS-generated 2D Lamb wave active sensing is illustrated step by step in Ref. [12]. In this study, the 2D analytical framework considering nonlinear wave damage interactions is emphasized and presented in details. FIGURE 1 shows the schematic of the proposed 2D analytical model. Lamb wave generation, propagation, nonlinear interaction with the damage (involving scattering, mode conversion, and higher harmonic generation), and reception are formulated using the exact analytical expressions. The analytical

model was constructed in frequency domain based on the exact 2D Lamb wave solution in the following steps:

STEP 1: Perform Fourier transform on the time-domain excitation signal $V_T(t)$ to obtain the frequency domain excitation spectrum $V_T(\omega)$.

STEP 2: Calculate structural transfer function. Detailed analytical derivation of 2D Lamb wave generated by a circular transmitter PWAS is given in Ref. [13]. And the structural transfer function can be separated into symmetric and antisymmetric parts, i.e.,

$$G^S(\omega,r) = -\pi i \frac{a^2 \kappa_{PWAS}(\omega)}{2\mu} \sum_{\zeta^S} \frac{J_1(\zeta^S a) N_S(\zeta^S)}{D_S^{'}(\zeta)} H_1^{(1)}(\zeta^S r) \quad (1)$$

$$G^A(\omega,r) = -\pi i \frac{a^2 \kappa_{PWAS}(\omega)}{2\mu} \sum_{\zeta^A} \frac{J_1(\zeta^A a) N_A(\zeta^A)}{D_A^{'}(\zeta)} H_1^{(1)}(\zeta^A r) \quad (2)$$

where a is the radius of the circular PWAS; $\kappa_{PWAS}(\omega)$ denotes the transducer transfer function, converting applied voltage into the shear stress, and the detailed formulation can be found in Ref [12]; μ denotes the shear modulus of the structure; ξ^S and ξ^A represent the wavenumbers of symmetric and antisymmetric modes, respectively; J_1 is the Bessel function of order one, which captures the tuning effect between PWAS and the host structure; $H_1^{(1)}$ is the Hankel function of the first kind and order one, which represents an outward propagating 2D wave field; ξ is the frequency dependent wavenumber calculated from the Reyleigh-Lamb equation; r is the distance between the point of interest and T-PWAS; the component functions of N_S, D_S, N_A, D_A can be referred to Ref [12].

STEP 3: Multiply the structural transfer function by the frequency-domain excitation signal to obtain the direct incident waves at the sensing location, where the distance R_{IN} from PWAS up to the sensing location is used. Similarly, multiply the structural transfer function up to the damage location by the frequency domain excitation signal to obtain the interrogating waves arriving at the damage, where the distance R_D from PWAS up to the damage location is used.

$$u_{IN}(\omega,R_{IN}) = V_T(\omega)[G^S(\omega,R_{IN}) + G^A(\omega,R_{IN})] \quad (3)$$

$$u_D(\omega,R_D) = V_T(\omega)[G^S(\omega,R_D) + G^A(\omega,R_D)] \quad (4)$$

where u_{IN} represents the frequency domain of the direct incident signal from the pristine path. It can be noticed that Lamb wave modes propagate independently and the direct incident wave field is the superposition of all wave modes.

STEP 4: In the damaged case, higher harmonic components may be produced due to the nonlinear wave crack interactions. The center frequency of the waves arriving at the nonlinear damage location can be obtained as f_c. The second and third higher harmonics are considered and act as new wave sources centered at $2f_c$ and $3f_c$, respectively. Modeling of higher harmonics is achieved by moving the frequency-domain signal at the damage location to the right-hand side of the frequency axis by f_c and $2f_c$, as is shown in FIGURE 1.

STEP 5: Scattering wave source at the damage location is obtained by modifying incident waves at the damage with the wave damage interaction coefficients (WDICs).

$$u_{NW}^S = \sum_{N=1}^{n} C_{SS}(\omega,\theta,N\omega_C) e^{-i\varphi_{SS}(\omega,\theta,N\omega_C)} u_D^S + \sum_{N=1}^{n} C_{AS}(\omega,\theta,N\omega_C) e^{-i\varphi_{AS}(\omega,\theta,N\omega_C)} u_D^A \quad (5)$$

$$u_{NW}^A = \sum_{N=1}^{n} C_{SA}(\omega,\theta,N\omega_C) e^{-i\varphi_{SA}(\omega,\theta,N\omega_C)} u_D^S + \sum_{N=1}^{n} C_{AA}(\omega,\theta,N\omega_C) e^{-i\varphi_{AA}(\omega,\theta,N\omega_C)} u_D^A \quad (6)$$

where u_{NW}^S and u_{NW}^A represent the damage scattered S0 and A0 wave sources, respectively. The general form of a nonlinear WDIC is given in the form of $C_{AB}(\omega,\theta,N\omega_C)e^{-i\varphi_{AB}(\omega,\theta,N\omega_C)}$, where A stands for the incident wave mode and B denotes the scatter wave mode. It should be noted that these WDICs are frequency, direction, and harmonic-order dependent, describing the amplitude and phase of the scattered waves as a function of frequency, direction, and different harmonic orders. It should be stated clearly that, in this study, our attention is focused on fundamental Lamb wave modes S0 and A0. Thus, $C_{SS}(\omega,\theta,N\omega_C)e^{-i\varphi_{SS}(\omega,\theta,N\omega_C)}$ represents the scattered symmetric mode generated from incident symmetric mode with the amplitude ratio $C_{SS}(\omega,\theta,N\omega_C)$ and the phase shift $e^{-i\varphi_{SS}(\omega,\theta,N\omega_C)}$ at N^{th} higher harmonic. Similarly, $C_{SA}(\omega,\theta,N\omega_C)e^{-i\varphi_{SA}(\omega,\theta,N\omega_C)}$ represents the scattered antisymmetric mode converted from an incident symmetric mode with the amplitude ratio $C_{SA}(\omega,\theta,N\omega_C)$ and the phase shift $e^{-i\varphi_{SA}(\omega,\theta,N\omega_C)}$. ω is the wave component frequency; θ represents the scattering angle with respect to the incident wave direction; N denotes the harmonic orders, and $N=1$ represents the linear wave-crack interaction; ω_C is the damaged structural angular frequency. From Eq. (5) and (6), it can observed that the nonlinear Lamb wave damage interaction involves scattering, mode conversion, and higher harmonic components. The final scattered field is the summation of different harmonic order scattered and mode converted waves. In this study, these WDICs are substituted by rational values, and the maximal third harmonic components is considered.

STEP 6: These scattered waves further propagate from the damage location to the sensing point. The scattered S0 and A0 waves arriving at the sensing point can be calculated.

$$u_{SC}^S = u_{NW}^S H_1^{(1)}(\xi^s R_{SC}) \quad (7)$$

$$u_{SC}^A = u_{NW}^A H_1^{(1)}(\xi^A R_{SC}) \quad (8)$$

where R_{SC} represents the distance from the damage up to the sensing location.

STEP 7: The total wave field at the sensing location is the superposition of the direct incident waves from Eq. (3) and the scattered waves calculated from Eq. (7) and Eq. (8), containing both linear and nonlinear components from wave damage interactions.

$$u_{TOTAL} = (u_{IN}^{S} + u_{IN}^{A}) + (u_{SC}^{S} + u_{SC}^{A}) \quad (9)$$

STEP 8: Perform inverse Fourier transform to obtain the time domain sensing signal.

$$u(t, R_D, R_{SC}) = IFFT[u(\omega, R_D, R_{SC})] \quad (10)$$

It should be noted that the total wave field obtain in Eq. (10) is the in-plane wave displacement. Corresponding transfer functions can be invoked to obtain sensing voltage at a receiver PWAS.

FIGURE 2 presents the 2D full-scale analytical model layout for the case study. The model is a 250 mm by 100 mm, 1-mm thick aluminum plate. The locations of the T-PWAS, general damage, and special recording points are illustrated. Both linear and nonlinear scattering effects may take place at the damage. A 3-count Hanning window modulated tone burst signal centered at 100 kHz is applied to the T-PWAS.

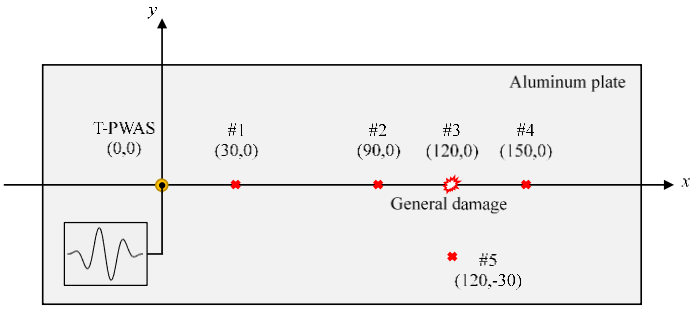

FIGURE 2: 2D FULL-SCALE ANALYTICAL MODEL LAYOUT FOR THE CASE STUDY

2.3 Lamb Wave Propagation in a Pristine Structure

FIGURE 3 shows the transient spatial field of wave propagation in a pristine aluminum plate. The yellow circle represents the 7-mm diameter T-PWAS. Lamb waves are generated by the T-PWAS, propagating out in a circular wave front, strong near the wave source, and weak at far field due to the outward propagation pattern. The S0 mode leads the way, propagating with faster speed and much longer wavelength than the A0 mode.

FIGURE 4 presents the sensing signals at various sensing locations in the pristine case. The S0 and A0 wave packages overlap with each other at location #1. From the waveforms at locations #2, #4, and #5, the A0 wave package clearly shows the dispersive characteristic. On the other hand, the S0 mode is much less dispersive than A0 mode, which almost retains the original excitation waveform.

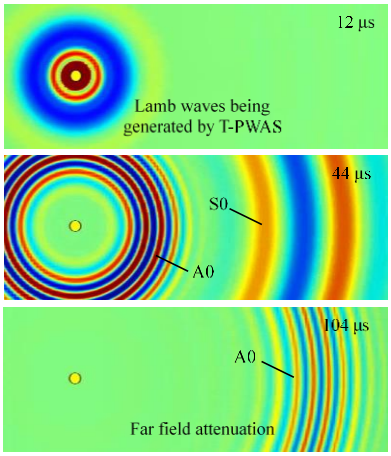

FIGURE 3: WAVE PROPAGATION IN A PRISTINE PLATE

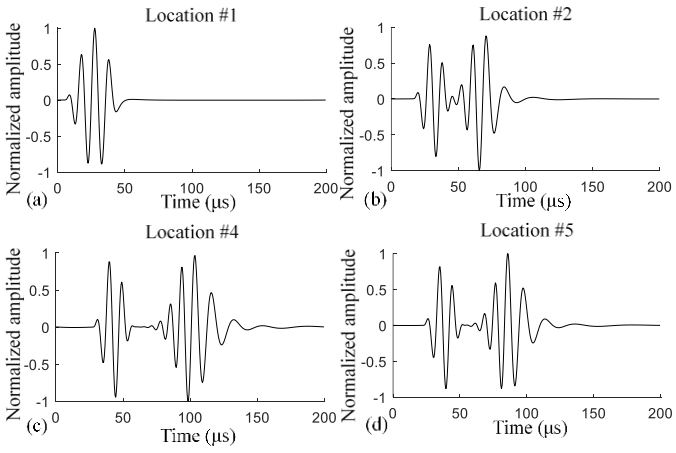

FIGURE 4: SENSING SIGNALS OF THE PRISTINE PLATE AT VARIOUS SENSING LOCATIONS: (A) SENSING SIGNAL AT LOCATION #1; (B) SENSING SIGNAL AT LOCATION #2; (C) SENSING SIGNAL AT LOCATION #4; (D) SENSING SIGNAL AT LOCATION #5

2.4 Linear Wave Damage Interaction Case

FIGURE 5 shows the transient spatial field of linear interactions between Lamb waves and the damage. The white circle represents a 4-mm diameter damage. When S0 waves interact with the damage, the mode converted A0 waves can be noticed, propagating with short wavelength. On the other hand, after A0 waves interact with damage, the scattered A0 mode can be observed as well as the shadings left behind the damage, which are caused by the destructive superposition between the incident A0 waves and the scattered A0 waves.

FIGURE 6 presents the sensing signals at various sensing locations of the linear wave damage interaction in both time domain and time-frequency domain. The sensing signals at locations #1 and #2 show that the scattered wave amplitude increases when the sensing location moves closer to the damage. The signals at locations #4 and #5 show the mode converted A0 wave package from the S0 interaction with damage. Furthermore, from the time-frequency domain signal, the contour areas only exist along 100 kHz around the excitation frequency. Especially, the signal at location #1 presents a single contour area, because both S0 and A0 modes almost arrive at the location at the same time. Besides, the scattered waves cannot be seen in the time-frequency domain because the energy of scattered waves are very weak compared with the direct incident waves. Furthermore, the temporal overlapping of the scattered wave field and the incident waves makes the identification even harder.

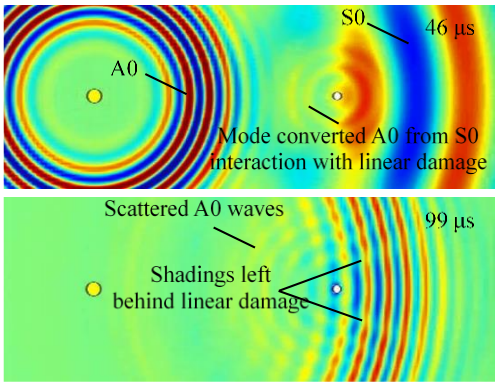

FIGURE 5: LINEAR INTERACTIONS BETWEEN LAMB WAVES AND THE STRUCTURAL DAMAGE

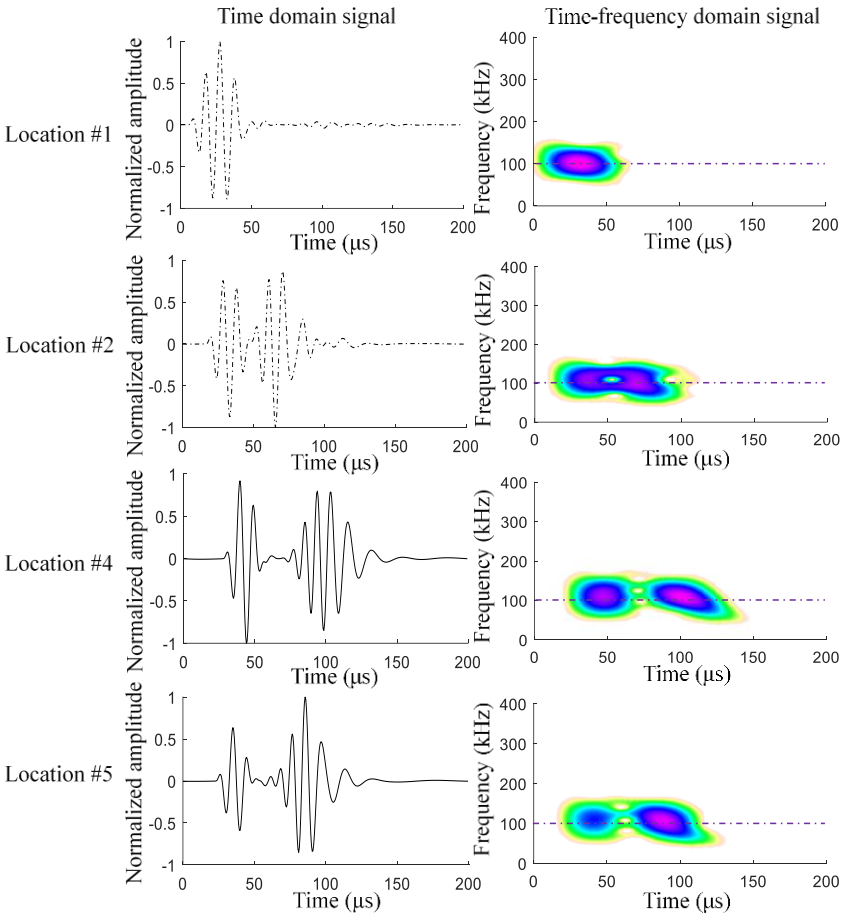

FIGURE 6: SENSING SIGNALS IN BOTH TIME DOMAIN AND TIME-FREQUENCY DOMAIN AT VARIOUS SENSING LOCATIONS OF THE LINEAR WAVE DAMAGE INTERACTION CASE

2.5 Nonlinear Wave Damage Interaction Case

FIGURE 7 presents the transient spatial field of nonlinear wave damage interaction for both S0 and A0 modes. When S0 mode interacts with the damage, S0 second harmonic component appears, as the wavelength of the scattered waves is approximately half of the wavelength of the fundamental S0 mode. In addition, after A0 mode interacts with the damage, wider spatial spread of scattered A0 waves can be observed compared with the linear wave damage interaction. It should be noted that the nonlinear interaction between guided waves and the damage becomes more complex as the second and third higher harmonic components are introduced.

FIGURE 8 shows the sensing signals in both time domain and time-frequency domain at various sensing locations of the nonlinear wave damage interaction case. From the time domain signals, many zigzags can be observed which represents the nonlinear effects. In addition, S0 waves carry more nonlinear features than A0 modes. This aspect can be equally demonstrated by the time-frequency analysis. Both second and third higher harmonic components exist in all the time-frequency domain signals, which cannot be found in the linear wave damage interaction case. Furthermore, the reflected nonlinear components can be recognized which apparently appears after the main wave packages at locations #1 and #2. On the other hand, the transmitted nonlinear response is much stronger than the reflected one, and the second harmonic response is much stronger than the third harmonic component.

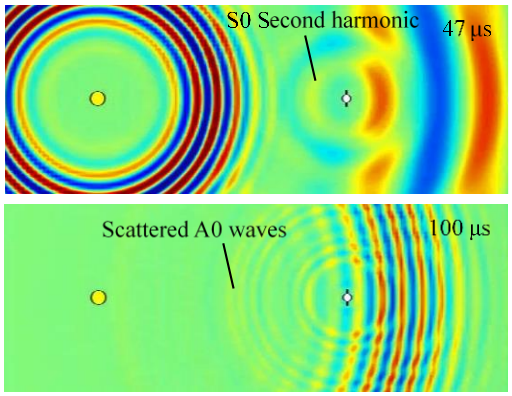

FIGURE 7: NONLINEAR INTERACTIONS BETWEEN LAMB WAVES AND THE STRUCTURAL DAMAGE

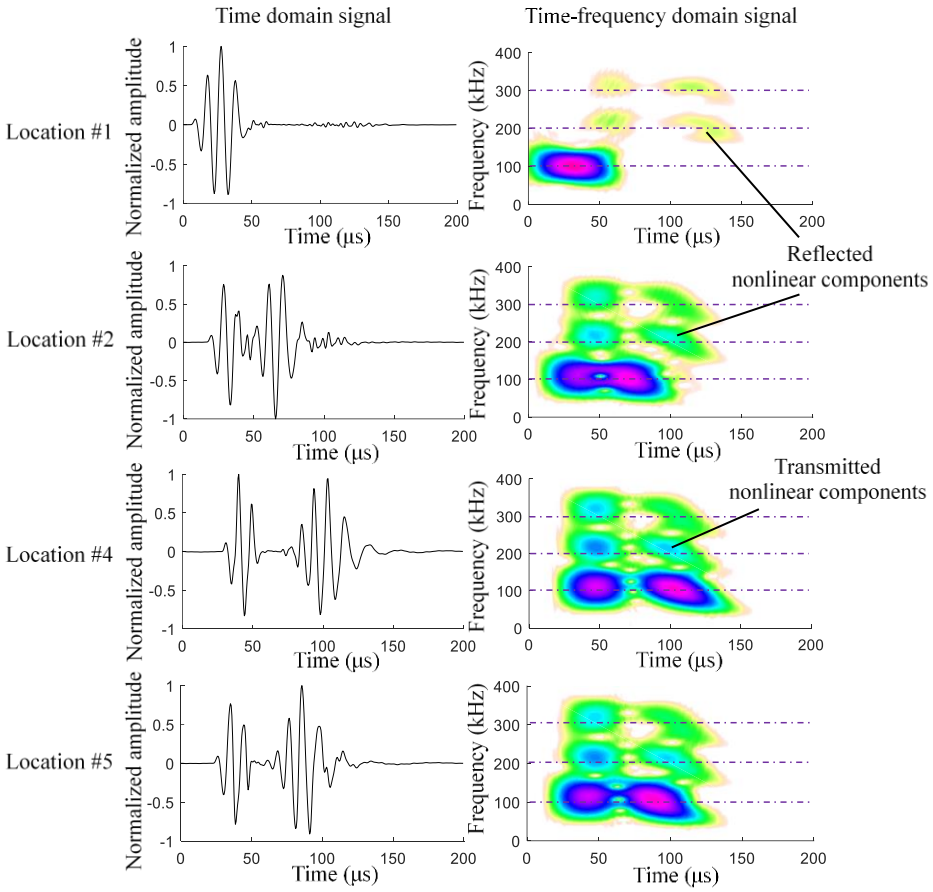

FIGURE 8: SENSING SIGNALS IN BOTH TIME DOMAIN AND TIME-FREQUENCY DOMAIN AT VARIOUS LOCATIONS FOR THE NONLINEAR WAVE DAMAGE INTERACTION CASE

3. NUMERICAL SIMULATION OF CONTACT ACOUSTIC NONLINAERITY DURING WAVE CRACK INTERACTION

This section illustrates the numerical study of Lamb wave generation, propagation, interaction with a fatigue crack, and reception. The pitch-catch procedure lays the foundation for the time reversing methods. This section emphasizes on the numerical modelling and simulation of Lamb waves interaction with the fatigue crack.

3.1 Finite Element Model

In this study, a 3D transient dynamic coupled-field finite element model was constructed to simulate the pitch-catch procedure in an aluminum plate with fatigue crack using ANSYS. Contact dynamics are considered to capture the nonlinear interactions between guided waves and the fatigue crack, which would induce CAN into the guided waves. Especially, to simulate the practical fatigue cracks, the rough contact condition was defined as well as the damping effect.

FIGURE 9 presents the finite element model with the fatigue crack. The model is a 1-mm thick aluminum plate with a 4-mm diameter rivet hole in the middle of the plate. The fatigue cracks were modeled nucleating from both sides of the hole with the length of 5 mm on each side. The transmitter and receiver PWAS were used for Lamb wave generation and reception, respectively. In addition, the distance between each PWAS and fatigue crack was 150 mm. The excitation frequency was carefully selected, where only single lamb wave mode was generated by the transmitter PWAS. According to Ref. [14], for a 1-mm thick aluminum plate, S0 mode dominates around 270 kHz, while A0 mode reaches its tuning point. Besides, the frequency bandwidth was kept as narrow as possible for better nonlinear phenomenon illustration. Furthermore, a rational choice of tone burst count number would relieve the computational load. Therefore, in this study, a 100 vpp 10-count Hanning window modulated sine tone burst signal centered at 270 kHz was applied on the T-PWAS. Non-reflective Boundaries (NRB) were implemented surrounding the entire plate. The length of NRB was adopted as 50 mm, twice as long as the wavelength of S0 mode at 270 kHz, which could guarantee the effective absorption of boundary reflections. To solve the problem accurately and efficiently, the mesh size and time step were optimized. The element size was set to 1 mm, which could guarantee enough points to depict up to the second higher frequency (540 kHz) wavelength. The time step was set to 0.1 μs, which can also satisfy the accuracy requirement of the second harmonic. In the thickness direction, the mesh size of 0.25 mm was adopted

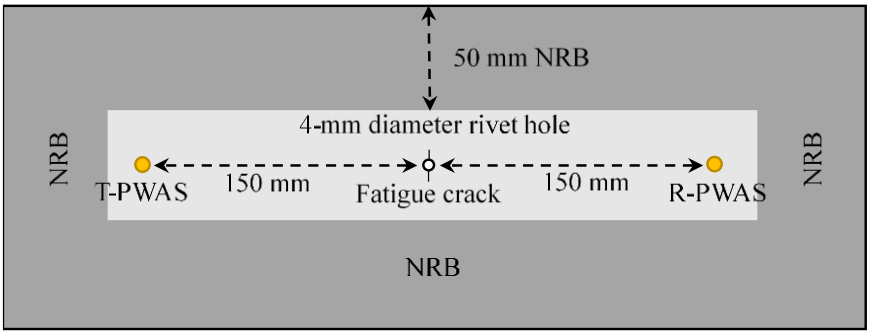

FIGURE 9: FINITE ELEMENT MODEL FOR WAVE PROAPGATION THROUGH A FATIGUE CRACK

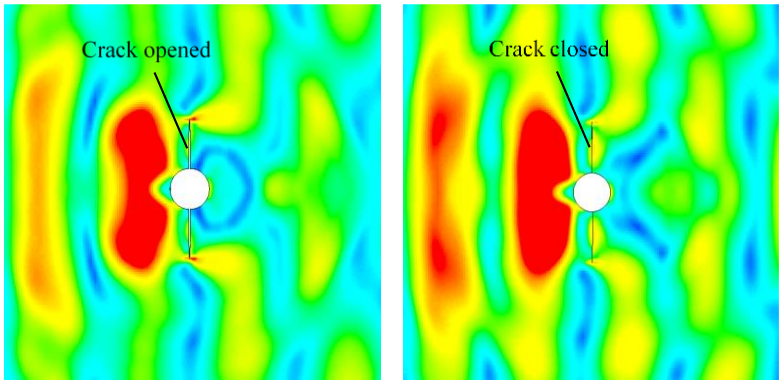

FIGURE 10: FATIGUE CRACK OPEN AND CLOSE CONTACT BEHAVIOR WHILE INTERACTING WITH INCIDENT LAMB WAVES: (A) S0 WAVE OPENED THE CRACK; (B) S0 WAVE CLOSED THE CRACK

3.2 Simulation Results

FIGURE 10 shows the simulation results for the nonlinear interaction between guided waves and the fatigue crack. Since S0 mode presents the tensile and compressive characteristics, it can produce crack open-close contact-impact phenomenon. When the tensile component interacts with the fatigue crack, the contact surfaces would separate from each other. On the other hand, for the compressive component, it causes the two contact surfaces collide with each other. It can be observed that high stress is produced during the crack close procedure due to the impact between the two contact surfaces. In addition, the tips of fatigue crack always possess comparative high stress concentration.

To better illustrate the nonlinear effect induced by the fatigue crack, the pristine model was also simulated with the same rivet hole in the middle of the plate, but without the fatigue cracks. Other aspects of the pristine model were all the same as the fatigue crack model. FIGURE 11 presents the sensing signals of the pristine and damaged cases in both time and frequency domain. From the time trace signals, the difference between both cases cannot be distinguished. However, the frequency spectra are totally different. The second and third higher harmonic components as well as the low frequency DC response can be clearly noticed. In contrast, there only exists the fundamental frequency peak in the pristine case. Therefore, the ultrasonic nonlinearity induced by the fatigue crack was demonstrated, which could be magnified after the time reversal procedure, involving a second time nonlinear interaction between the reversed Lamb wave and the fatigue crack.

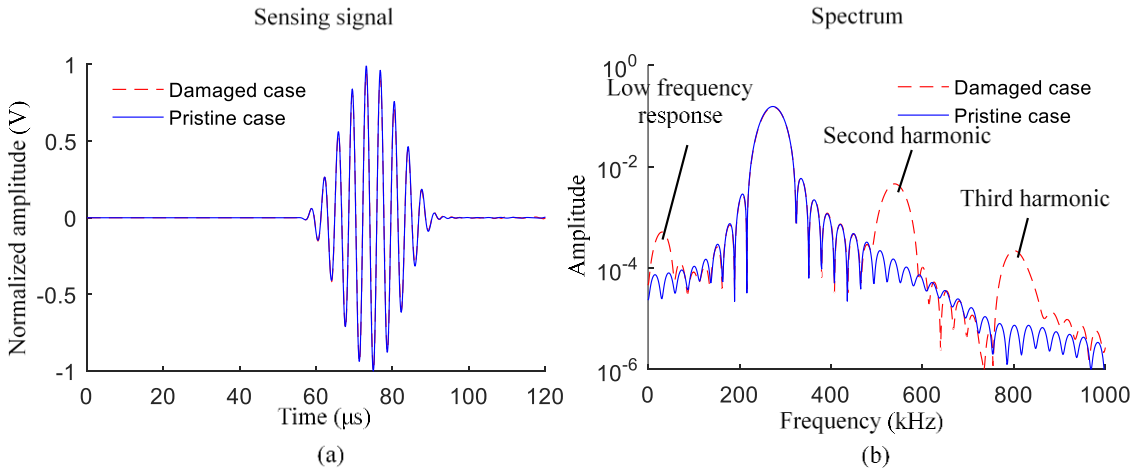

FIGURE 11: SENSING SIGNALS OF PRISTINE AND DAMAGED CASES: (A) TIME TRACE OF SENSING SIGNALS; (B) FREQUENCY SPECTRA OF SENSING SIGNALS

4. NONLINEAR LAMB WAVE TIME REVERSING

4.1 Virtual Time Reversal Algorithm

The VTR algorithm has widely been utilized for damage detection in SHM and Non-destructive Evaluation (NDE) communities [3, 4]. However, it has not been investigated for the nonlinear damage detection scenario. This study strives to research on the VTR algorithm for fatigue crack detection. The theoretical fundamentals can be found in Ref. [3]

$$V_C(\omega) = V_R^*(\omega)\frac{V_R(\omega)}{V_T(\omega)} \tag{11}$$

where $V_T(\omega)$ is the excitation waveform in the frequency domain; $V_R(\omega)$ represents the pitch-catch signal in the frequency domain; $V_C(\omega)$ denotes the reconstructed signal in the frequency domain; the superscript * denotes a complex conjugate processing, facilitating the time reversal operation of a signal in the frequency domain. In this study, only the transmitted S0 mode is considered. The influence affected by the nonlinear interaction between guided waves and the fatigue crack will be illustrated in the following text.

4.2 Damage Indices

In this research, two DIs are used. The first one is to compare the reconstructed signal and excitation waveform, which can be referred in Ref. [3]

$$DI_1 = 1 - \frac{\left|\int_{t_0}^{t_1} I(t)V(t)dt\right|}{\sqrt{\int_{t_0}^{t_1} I^2(t)dt \int_{t_0}^{t_1} V^2(t)dt}} \tag{12}$$

where $I(t)$ represents the excitation signal; $V(t)$ denotes the reconstructed signal for either traditional time reversal or virtual time reversal procedures; t_0 and t_1 represent the starting and ending time instance of the input tone burst signal. The other one is to compare the frequency response between the fundamental frequency and second higher harmonic, after Ref. [9], i.e.

$$DI_2 = \frac{|A(2\omega)|}{|A(\omega)|} \tag{13}$$

where $|A(\omega)|$ represents the spectral magnitude of the fundamental frequency and $|A(2\omega)|$ denotes the magnitude of

the second harmonic of the reconstructed signal. These two DIs can illustrate the time reversibility of the active sensing signals while nonlinear interactions between guided waves and the fatigue crack take place. They can either work independently or be casted into a fused DI for the detection and quantitative evaluation of the fatigue crack.

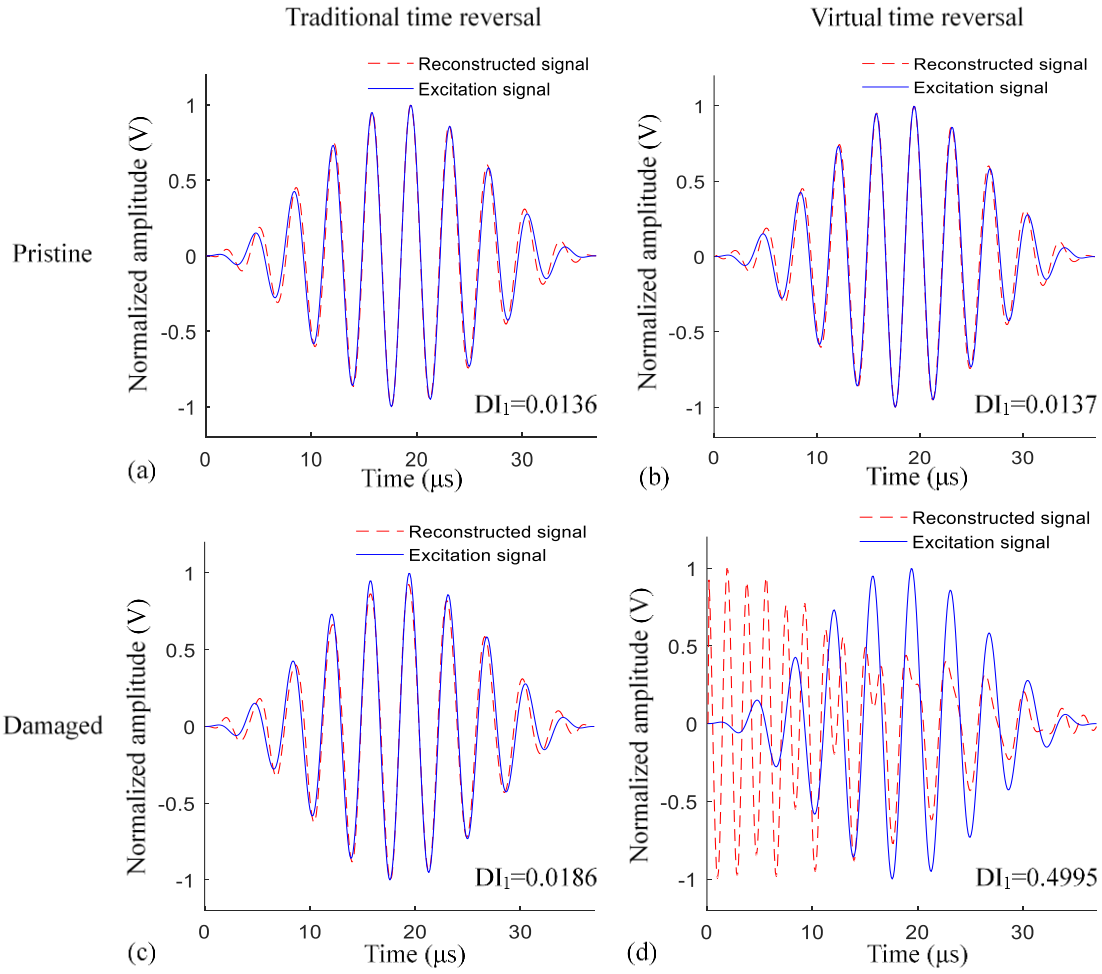

FIGURE 12: RECONSTRUCTED SIGNALS USING TRADITIONAL AND VIRTUAL TIME REVERSAL ALGORITHM FOR PRISTINE AND DAMAGED CASES: (A) PRISTINE CASE SIGNAL FROM TRADITIONAL TIME REVERSAL METHOD; (B): PRISTINE CASE SIGNAL FROM VIRTUAL TIME REVERSAL METHOD; (C) DAMAGED CASE SIGNAL FROM TRADITIONAL TIME REVERSAL METHOD; (D) DAMAGED CASE SIGNAL FROM VIRTUAL TIME REVERSAL METHOD

4.3 Time Reversal Results

Both the traditional time reversal procedure and virtual time reversal algorithm were conducted for fatigue crack detection. The traditional time reversal procedure was achieved as follows: after the first round of forward pitch-catch active sensing, the received signal was time-reversed and reemitted back from the original R-PWAS. The backward pitch-catch procedure would then take place. The original T-PWAS, this time, served as the receiver and picked up the sensing signal. Finally, the sensing signal was time reversed again and compared with the excitation. On the other hand, as only the excitation signal and pitch-catch sensing signal are needed in the virtual time reversal algorithm, the reconstructed signal can be obtained according to Eq. (11) for the VTR method. FIGURE 12 shows the reconstructed signals for the pristine and damaged cases, and FIGURE 13 presents the frequency spectra of the reconstructed signals from the traditional time reversal procedure and VTR algorithm. In the pristine case, the difference between the reconstructed signal and excitation signal is small for both traditional time reversal procedure and VTR algorithm. And the DI results are almost the same in both time and frequency domain. However, for the damaged case, the reconstructed signal of traditional time

reversal method does not change much compared with the pristine case, even though the second and third higher harmonic components exist in the frequency spectrum. But for the virtual time reversal results, apparent amplitude and phase mismatch can be noticed in FIGURE 12d. Relating to the frequency spectrum in FIGURE 13d, the amplitude of second harmonic even exceed that of fundamental frequency, as the ratio approximates 3. As a consequence, in the very beginning of the reconstructed signal, half-period oscillation signal can be observed (corresponding to the second harmonic component), followed by the fundamental frequency vibration waveform. In addition, the oscillation amplitude decreases as time elapses. From Eq. (11), it can be noticed that the excitation signal is divided by the pitch-catch signal in the frequency domain. On the other hand, the second harmonic in the frequency spectrum of the excitation signal is quite small compared with the fundamental frequency, Therefore, after division, the second harmonic component of the reconstructed signal is artificially magnified, which can even overpass the amplitude of fundamental frequency. In conclusion, the virtual time reversal algorithm can highlight the nonlinear components in the frequency spectrum of the pitch-catch signal. It may possess the better diagnostic ability for fatigue crack detection compared with the traditional time reversal method.

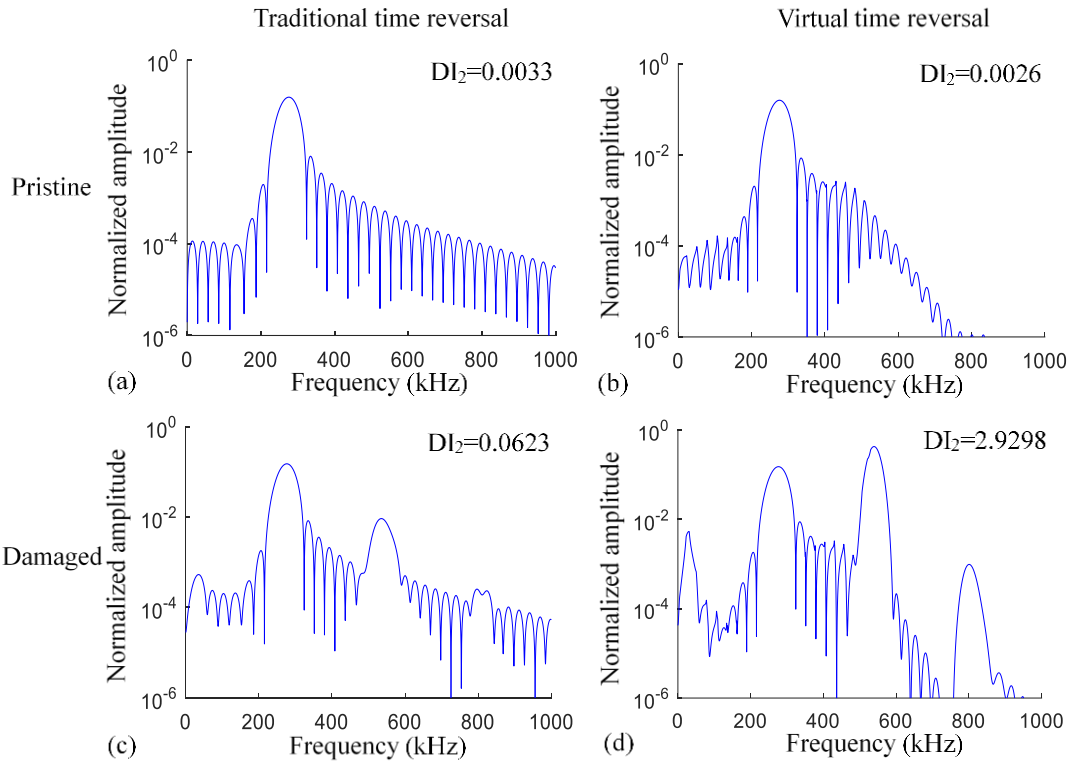

FIGURE 13: FREQUENCY SPECTRUM OF RECONSTRUCTED SIGNALS FOR BOTH TRADITIONAL AND VIRTUAL TIME REVERSAL ALGORITHM: (A) PRISTINE SPECTRUM OF TRADITIONAL TIME REVERSAL; (B) PRISTINE SPECTRUM OF VIRTUAL TIME REVERSAL; (C) DAMAGED SPECTRUM OF TRADITIONAL TIME REVERSAL; (D) DAMAGED SPECTRUM OF VIRTUAL TIME REVERSAL

5. CONCLUDING REMARKS

This paper presented a numerical study on nonlinear Lamb wave time reversing for fatigue crack detection. The 2D analytical model was constructed for the efficient simulation of Lamb wave generation, propagation, linear and nonlinear wave damage interaction, and reception. The scattering, mode conversion, higher harmonic phenomena can be apparently noticed from the analytical simulation results.

A 3D transient dynamic coupled-field finite element model was constructed to simulate the pitch-catch procedure in an aluminum plate with fatigue cracks. The fatigue cracks were modelled nucleating from both sides of a rivet hole. Based on the pitch-catch procedure, single S0 mode time reversal procedure was simulated for both the pristine and the damage cases.

By comparing the results of nonlinear traditional time reversal method and nonlinear virtual time reversal algorithm, the nonlinear virtual time reversal algorithm can better diagnose the presence of the fatigue crack. As the higher harmonic component dominates the frequency spectrum, the time reversibility was clearly broken. On the other hand, the nonlinear

time reversal method can still serve as a baseline-free damage detection for fatigue crack with incremental feature changes in both time and frequency domain.

The analytical solutions and finite element simulation are expected to be validated by the experimental demonstration in the future work.

ACKNOWLEDGEMENTS

This work was sponsored by the National Natural Science Foundation of China (Contract Number: 51605284).

REFERENCES

[1] K. Y. Jhang, "Nonlinear ultrasonic techniques for nondestructive assessment of micro damage in material: A review," *International Journal of Precision Engineering & Manufacturing,* vol. 10, no. 1, pp. 123-135, 2009.

[2] Y. Shen, J. Wang, and W. Xu, "Nonlinear features of guided wave scattering from rivet hole nucleated fatigue cracks considering the rough contact surface condition," *Smart Materials and Structures,* vol. 27, no. 10, 2018.

[3] Z. Liu, H. Yu, J. Fan, Y. Hu, C. He, and B. Wu, "Baseline-free delamination inspection in composite plates by synthesizing non-contact air-coupled Lamb wave scan method and virtual time reversal algorithm," *Smart Materials and Structures,* vol. 24, no. 4, 2015.

[4] J. Wang and Y. Shen, "Lamb wave virtual time reversal damage detection algorithm with transducer transfer function compensation," in *2019 SPIE Smart Structures and NDE*, Denver, Colorado, USA, 2019.

[5] J. Wang and Y. Shen, "Numerical Investigation of Ultrasonic Guided Wave Dynamics in Piezoelectric Composite Plates for Establishing Structural Self-Sensing," *Journal of Shanghai Jiaotong University (Science),* vol. 23, no. 1, pp. 175-181, 2018.

[6] T. J. Ulrich, A. M. Sutin, T. Claytor, P. Papin, P.-Y. Le Bas, and J. A. TenCate, "The time reversed elastic nonlinearity diagnostic applied to evaluation of diffusion bonds," *Applied Physics Letters,* vol. 93, no. 15, 2008.

[7] S. Vejvodova, Z. Prevorovsky, and S. Dos Santos, "Nonlinear Time Reversal Tomography of Structural Defects," 2009.

[8] E. Barbieri and M. Meo, "Discriminating linear from nonlinear elastic damage using a nonlinear time reversal DORT method," *International Journal of Solids and Structures,* vol. 47, no. 20, pp. 2639-2652, 2010.

[9] P. Blanloeuil, L. R. F. Rose, M. Veidt, and C. H. Wang, "Time reversal invariance for a nonlinear scatterer exhibiting contact acoustic nonlinearity," *Journal of Sound and Vibration,* vol. 417, pp. 413-431, 2018.

[10] M. Hong, Z. Su, Y. Lu, H. Sohn, and X. Qing, "Locating fatigue damage using temporal signal features of nonlinear Lamb waves," *Mechanical Systems and Signal Processing,* vol. 60-61, pp. 182-197, 2015.

[11] Y. Shen and V. Giurgiutiu, "WaveFormRevealer: An analytical framework and predictive tool for the simulation of multi-modal guided wave propagation and interaction with damage," *Structural Health Monitoring: An International Journal,* vol. 13, no. 5, pp. 491-511, 2014.

[12] Y. Shen and V. Giurgiutiu, "Combined analytical FEM approach for efficient simulation of Lamb wave damage detection," *Ultrasonics,* vol. 69, pp. 116-28, Jul 2016.

[13] V. Giurgiutiu, *Structural Health Monitoring with Piezoelectric Wafer Active Sensors*, second Edition ed. Elsevier Academic Press, 2014.

[14] B. Xu and V. Giurgiutiu, "Single Mode Tuning Effects on Lamb Wave Time Reversal with Piezoelectric Wafer Active Sensors for Structural Health Monitoring," *Journal of Nondestructive Evaluation,* vol. 26, no. 2-4, pp. 123-134, 2007.